International Journal of Modern Physics C
Vol. 18, No. 2 (2007) 203–216

World Scientific
www.worldscientific.com

COMPARISON OF GAS SLIP MODELS WITH SOLUTIONS OF LINEARIZED BOLTZMANN EQUATION AND DIRECT SIMULATION OF MONTE CARLO METHOD

G. H. TANG*, Y. L. HE and W. Q. TAO

State Key Laboratory of Multiphase Flow
School of Energy and Power Engineering
Xi'an Jiaotong University, Xi'an, 710049, China
**ghtang@mail.xjtu.edu.cn*

Received 13 March 2006
Accepted 24 April 2006

Analytical solutions of the Navier–Stokes equation based on a locally fully-developed flow assumption with various gas slip models are presented and comparisons for velocity profile, flow rate, friction factor, and pressure distribution are performed. The effect of the second-order coefficient in the slip boundary condition becomes significant as the Knudsen number increases. Most slip models are limited to slip regime or marginally transition regime and break down around $Kn = 0.1$ while Sreekanth's model, followed by Mitsuya's model, gives a good agreement with the linearized Boltzmann solutions from slip regime up to $Kn = 2$ for flow rate and friction factor predictions. These two models should be of great use for slip flow analysis in micro-electro-mechanical systems (MEMS) and, in particular, in situations where the flow rate and flow resistance are of interest.

Keywords: Slip flow; Knudsen number; Navier–Stokes equation; slip model.

PACS Nos.: 47.45.Gx, 47.11.-j, 47.45.-n.

1. Introduction

The recent rapid development of microfabrication technologies has made increasing applications for fluid microsystems in various fields.[1] To meet this demand, a deep understanding of the flow and heat transfer in microscale is very important and urgent. As the scale of the domain is reduced, the continuum assumption may no longer be applicable. Some effects that are typically neglected at the macroscale must be included in the analysis of microscale problems. One such condition is the slip velocity at the solid surfaces. The Knudsen number, Kn, the ratio of the gas mean free path λ to the characteristic dimension h of the flow, provides a direct means of validating the continuum approach. Generally, for $Kn > 0.001$, the classical boundary conditions of no-slip velocity and no-jump temperature at solid boundaries break down.

Experimental studies for the flow measurements in microchannels have been conducted and the results are quite contradictory. For example, the measured friction factors by Wu and Little[2] are much higher than those predicted by the conventional theory, while the friction factors measured in Refs. 3–5 are lower than the conventional ones. One reason accounting for the contradictory test results in the friction factor is associated with the obvious measurement difficulties. Numerical analysis, however, provides an alternative and effective way for investigating the flow inside a microchannel or a more complex geometry.

A number of theoretical researches using analytical and numerical methods have been carried out to study the rarefaction effect on gaseous flow characteristics. Analytical models by solving the Navier–Stokes equation with first-order slip boundary conditions (Maxwell slip boundary conditions) have been developed by Kennard,[6] Burgdorfer,[7] Ebert and Sparrow,[8] Arkilic *et al.*,[9] Morini and Spiga,[10] and Sun and Faghri.[11] Second-order slip models have been developed by Schamberg,[12] Cercignani,[13] Deissler,[14] Sreekanth,[15] Hisa and Domoto,[16] Mitsuya,[17] Beskok and Karniadakis,[18] Aubert and Colin,[19] Hadjiconstantinou,[20] and Maurer *et al.*[21]

Numerical methods for solving the Navier–Stokes equations together with the first-order or second-order slip-velocity boundary conditions, such as the finite volume method (FVM) and the finite difference method (FDM), can be found in Refs. 22–29. Furthermore, Xue *et al.*[30,31] numerically solved the Burnett equation with first-order slip boundary conditions for micro-Couette flow. Recently, Du and Suzuki[32] studied the turbulent microscale characteristics using the direct numerical simulation method (DNS). However, the computation effort for the DNS method is rather heavy compared to the methods by numerically solving the Navier–Stokes equations. More recently the lattice Boltzmann method (LBM) has also been developed for microflows.[33–38] The advantage of LBM is its convenient applications for complex geometries and parallel computing.

The linearized Boltzmann equation[39–41] or BGK equation[42] is suitable for solving the low speed rarefied gas flows and its solutions for benchmark problems may serve as criteria for testing other methods. But the complexity in performing the numerical solution of the Boltzmann equation or BGK equation limits most existing solutions to simple geometries such as parallel plates or cylinder tubes.

The direct simulation of Monte Carlo (DSMC) method, a molecular-based model, is often applied to investigate low-pressure rarefied gas flow characteristics[43] and can be applied to any complex geometric problems. The DSMC method, however, needs much computational effort to obtain the results of desired accuracy, which makes the simulation go to easily beyond the capabilities of most computers.

In summary, accurate second-order slip models are highly desirable because they allow the solution of flow problems using the continuum description that is significantly more efficient compared to molecular-based approaches.[20] For this reason, we summarize and evaluate various first-order and second-order slip models in this paper and attempt to provide advice for readers when employing the slip models, especially from the view of engineering applications. The following sections are

organized as follows. First, analytical solutions for the Navier–Stokes equation with slip boundary conditions are briefly presented. Then, the results of velocity, flow rate, friction factor, and pressure distribution for various slip models are discussed and compared with the solutions of linearized Boltzmann equation and DSMC method. Finally, the conclusions are made.

2. Analytical Solutions for Isothermal Gaseous Flow with Slip Boundary Conditions

Consider a two-dimensional steady and isothermal gas flow between two fixed parallel plates. The channel with the height of h extends from $y = 0$ to $y = h$. Based on the locally fully developed flow assumption,[8] the momentum equation in the Cartesian coordinate system becomes,

$$\frac{\partial^2 u}{\partial y^2} = \frac{1}{\eta}\frac{dp}{dx}\,. \tag{1}$$

The second-order velocity slip boundary condition usually has the following form

$$u - u_w = \pm C_1 \lambda \frac{\partial u}{\partial y} - C_2 \lambda^2 \frac{\partial^2 u}{\partial y^2}\,, \tag{2}$$

where u is the gas slip velocity near the wall, u_w is the tangential velocity of the wall ($u_w = 0$ for fixed walls), and y is the coordinate normal to the wall. It is noted that all the discussion in this study are based on diffusive reflection, i.e., the tangential momentum accommodation coefficient $\sigma_\nu = 1$. C_1 and C_2 are constants denoting the first-order term and second-order term, respectively. Equation (2) recovers Maxwell velocity slip boundary condition if $C_2 = 0$. The values of C_1 and C_2 proposed by various authors are summarized in Table 1. Thereinto, in Hadjiconstantinou's model, $C_2 = 0.61$ is used for local velocity distribution and $C_2 = 0.31$ for mean velocity and friction factor.

Table 1. First-order and second-order coefficients for various slip models.

Author	C_1	C_2
Maxwell (Kennard, 1938)	1.0	0
Schamberg (1947)	1.0	$5\pi/12$
Cercignani (1964)	1.1466	0.9756
Deissler (1964)	1.0	9/8
Sreekanth (1969)	1.1466	0.14
Hisa and Domoto (1983)	1.0	0.5
Mitsuya (1993)	1.0	2/9
Beskok and Karniadakis (1994)	1.0	−0.5
Hadjiconstantinou (2003)	1.11	0.61 (0.31)

Integrating Eq. (1) twice and adopting the boundary conditions, Eq. (2), we can obtain the following analytical solution:

$$u = -\frac{h^2}{2\eta}\frac{dp}{dx}\left(\frac{y}{h} - \frac{y^2}{h^2} + C_1 Kn + 2C_2 Kn^2\right), \tag{3}$$

where the Knudsen number is defined as $Kn = \lambda/h$ and η is the fluid dynamic viscosity. We have

$$\lambda = \frac{\eta}{p}\sqrt{\frac{\pi RT}{2}}. \tag{4}$$

A further integration in y-direction results in an expression for the average velocity, u_A, in the channel:

$$u_A = -\frac{h^2}{2\eta}\frac{dp}{dx}\left(\frac{1}{6} + C_1 Kn + 2C_2 Kn^2\right) \tag{5}$$

Then, we can obtain

$$\frac{u}{u_A} = \frac{y/h - y^2/h^2 + C_1 Kn + 2C_2 Kn^2}{1/6 + C_1 Kn + 2C_2 Kn^2}. \tag{6}$$

For comparison with the solutions of the linearized Boltzmann equation, a non-dimensional flow rate Q_A is introduced[44]

$$Q_A = \frac{u_A}{-(h/p)(dp/dx)\sqrt{(RT/2)}} = \frac{\sqrt{\pi}(1 + 6C_1 Kn + 12C_2 Kn^2)}{12Kn}. \tag{7}$$

Based on the ideal gas flow assumption $p = \rho RT$ and $pKn = p_0 Kn_0$ (p_0 is the outlet gas pressure), we can obtain, omitting the derivation process for brevity, the mass flow rate through the channel,

$$\dot{m} = \rho h u_A = \frac{p_0^2 h^3}{24RT\eta L}(\Pi^2 - 1 + 12C_1 Kn_0(\Pi - 1) + 24C_2 Kn_0^2 \ln\Pi), \tag{8}$$

where $\Pi = p_i/p_0$ denotes the pressure ratio of the channel inlet to the outlet. Having obtained the mass flow rate, the corresponding pressure distribution along the channel can be obtained as

$$P^2 - \Pi^2 + 12C_1 Kn_0(P - \Pi) - 24C_2 Kn_0^2 \ln\left(\frac{\Pi}{P}\right) - [1 - \Pi^2 + 12C_1 Kn_0(1 - \Pi) - 24C_2 Kn_0^2 \ln\Pi]\frac{x}{L} = 0, \tag{9}$$

where L is the channel length, and the subscripts "i" and "o" denote the inlet and outlet of the channel, respectively. Here we define $P = p/p_0$, i.e., the local pressure at a station x normalized with the outlet pressure.

The shear stress τ_w can be obtained as follows

$$\tau_w = \eta\left(\frac{\partial u}{\partial y}\right)_{y=0} = -\frac{h}{2}\frac{dp}{dx}. \tag{10}$$

Then, the local friction factor can be obtained from the pressure distribution in the following form,

$$C_f = \frac{\tau_w}{\rho u_A^2/2} = \frac{24}{\mathrm{Re}(1 + 6C_1 Kn + 12C_2 Kn^2)} = \frac{2\sqrt{\pi}}{\mathrm{Re}KnQ_A}\,, \tag{11}$$

where the Reynolds number is defined as $\mathrm{Re} = 2\rho u_A h/\eta$.

3. Results and Discussion

In Fig. 1, we compare velocity distribution obtained by various slip boundary conditions with the linearized Boltzmann solutions.[40] The plotted velocity is normalized with the local average velocity, u_A. The corresponding deviations from the linearized Boltzmann solutions are also shown in the figures. The error is positive if the slip model over-predicts the velocity at a given point and is negative if the velocity is under-predicted. For slip velocity prediction at wall the model of Beskok and Karniadakis with the smallest second-order coefficient ($C_2 = -0.5$) gives the best agreement with the linearized Boltzmann solutions, followed by Maxwell's model ($C_2 = 0$), while Cercignani's boundary condition performs the worst for $Kn = 0.1128$ and Hadjiconstantinou's model and Schamberg's model perform the worst for the other larger Knudsen numbers. This can be explained as follows. The first-order coefficient dominates the slip velocity for lower Knudsen numbers while the second-order coefficient plays a more important role for higher Knudsen numbers. From Table 1 we can see that the first-order coefficient of Schamberg's model ($C_1 = 1.0$) is a little smaller than that of Cercignani's model ($C_1 = 1.1466$) while the second-order coefficient of Schamberg's model ($C_2 = 5\pi/12$) is larger than that of Cercignani's ($C_2 = 0.9756$). Maxwell's model and Beskok and Karniadakis's model give the most accurate description of the centerline velocity, while Cercignani's model and Schamberg's model once again perform the worst. From the figure we can also see that the slip models with positive second-order slip coefficients ($C_2 > 0$) under-estimate the centerline velocity while the slip model with $C_2 < 0$ over-estimates the centerline velocity in the shown Knudsen number range with the exception of Hadjiconstantinou's model.

From Eq. (5) we can see that a positive second-order coefficient gives enhancement of the flow rate while a negative second-order coefficient gives a reduction compared to the Maxwell's boundary predictions. The non-dimensional flow rate Q_A presented in Fig. 2 also demonstrates this argument. The predictions from all the slip models and the linearized Boltzmann solutions are in rough agreement when $Kn < 0.1$. Significant discrepancy occurs for $Kn > 0.1$. However, the predictions from Sreekanth' model ($C_2 = 0.14$), followed by Mitsuya's model ($C_2 = 2/9$) agree well with the linearized Boltzmann solutions up to $Kn = 2$. The other models with $C_2 > 0$ give an obvious increase while the slip models of Beskok and Karniadakis ($C_2 = -0.5$), and Maxwell ($C_2 = 0$) give obvious reduction compared to the linearized Boltzmann solutions for $Kn > 0.1$. The prediction of Schamberg's model, which has the largest second-order coefficient, gives the largest deviation to the

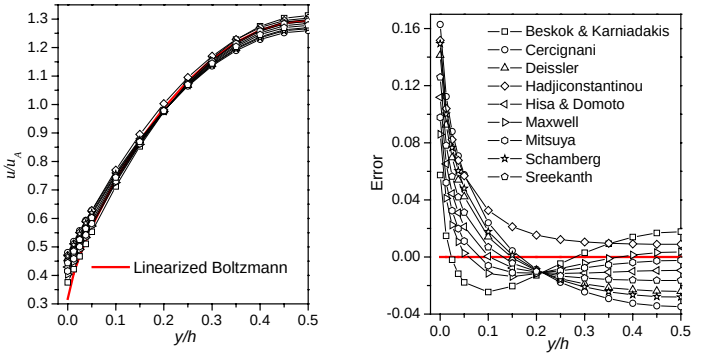

(a)

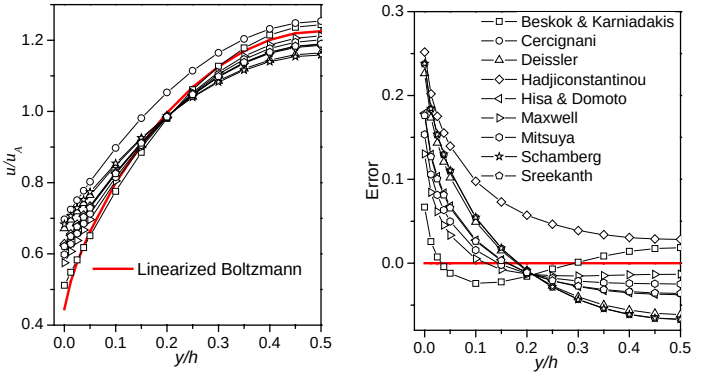

(b)

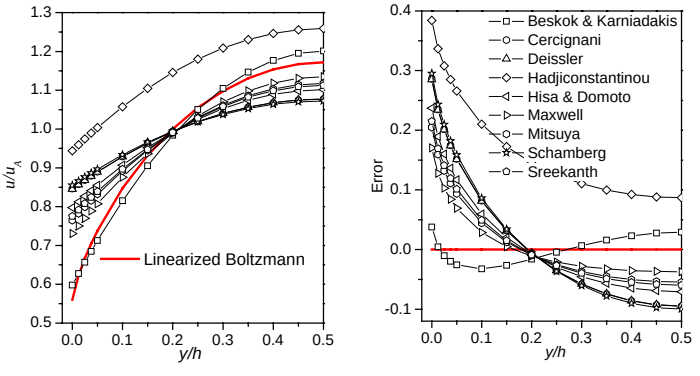

(c)

Fig. 1. The velocity distribution normalized with the local average velocity in the microchannel (left). Errors in the solution of the Navier–Stokes equation with various slip models (right). The meanings of the various symbols are demonstrated in the figure. The solid line denotes the linearized Boltzmann solutions from Ref. 40. (a) $Kn = 0.1128$, (b) $Kn = 0.2257$ and (c) $Kn = 0.4513$.

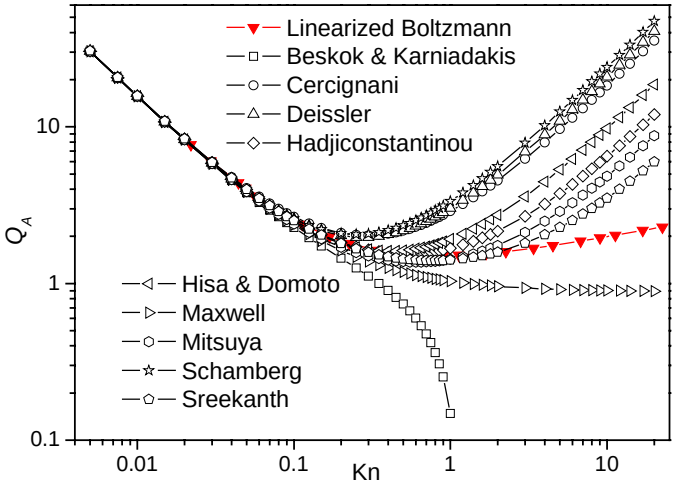

Fig. 2. Comparison of non-dimensional flow rate Q_A resulting from each slip model.

higher side while Beskok and Karniadakis's model gives the largest deviation to the lower side.

The friction factors are shown in Fig. 3. Here, the comparisons are based on the following friction factor expression given by Hadjiconstantniou.[44]

$$C_f = \frac{32}{5\sqrt{\pi}\mathrm{Re}KnQ_A}\,, \tag{12}$$

where Q_A is determined by the linearized Boltzmann solutions. It is noted that here Hadjiconstantniou used another type of viscosity-based mean free path and the expression of Eq. (12) differs from Eq. (11) only by 2%. Corresponding to the flow rate results, from Fig. 3 we can see that the friction factors from Schamberg's model have the largest deviation on the low side from the predictions of Eq. (12) while the ones from Beskok and Karniadakis's model have the largest deviation on the high side. The Sreekanth's model, followed by Mitsuya's model, gives predictions closest to the results of Eq. (12) up to $Kn = 2$.

The mass flow rate predictions in pressure driven microchannels from various slip models are compared with the available experimental data[45–47] in Fig. 4. We can see that the discrepancy among the slip models is very small for $Kn < 0.1$ while the discrepancy gets larger for higher Knudsen numbers or larger pressure ratios. For the case of helium gas flow [Fig. 4(a)], compared with the experimental data, Cercignani's model gives the largest deviation on the high side, while Beskok and Karniadakis's model gives the largest deviation on the low side. Rather, the deviation increases as the pressure ratio increases. Similarly, the predictions from Sreekanth's model and Mitsuya's model are in quite good agreement with the experimental data within the present Knudsen number and pressure ratio ranges.

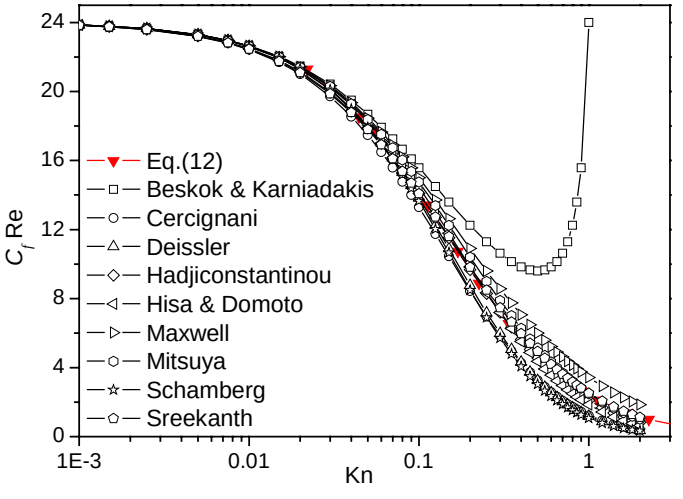

(a)

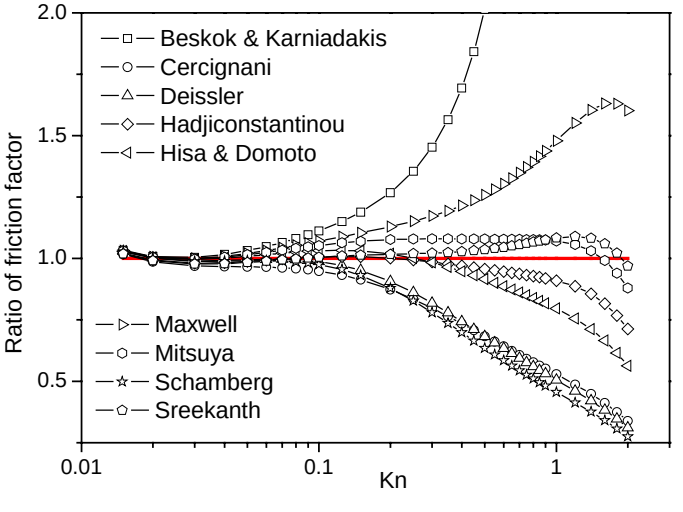

(b)

Fig. 3. Comparison of friction constant C_fRe resulting from each slip model. (a) C_fRe versus Kn and (b) The friction factor ratio of predictions from various slip models to Eq. (12).

We also examine the pressure distribution from various slip models by plotting the curvature in pressure distribution, i.e., the deviation from the corresponding linear pressure drop for an incompressible flow, p_{lin}. From Fig. 5 we can see that the curvature in pressure distribution decreases as the second-order coefficient increases. Schamberg's model with the largest second-order coefficient gives the lowest

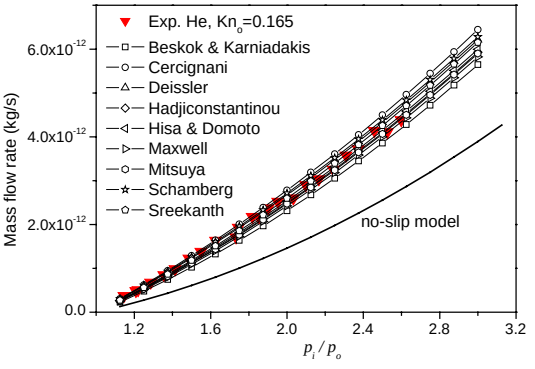

(a)

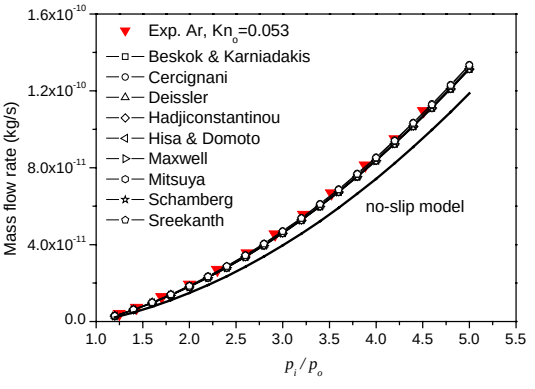

(b)

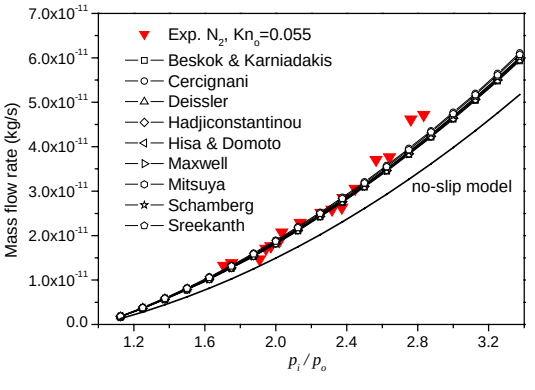

(c)

Fig. 4. Comparison of mass flow rate between the predictions of various slip models and the available experimental data. (a) $Kn_0 = 0.165$, helium gas flow. The experimental data are from Ref. 45, (b) $Kn_0 = 0.053$, argon gas flow. The experimental data are from Ref. 46 and (c) $Kn_0 = 0.055$, nitrogen gas flow. The experimental data are from Ref. 47.

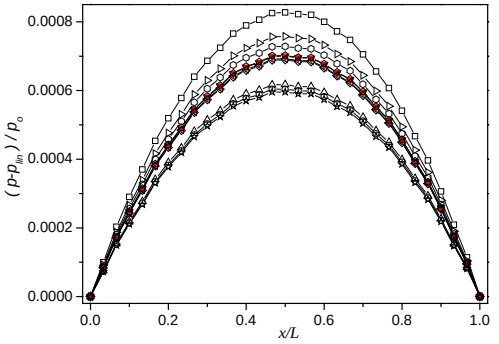

(a)

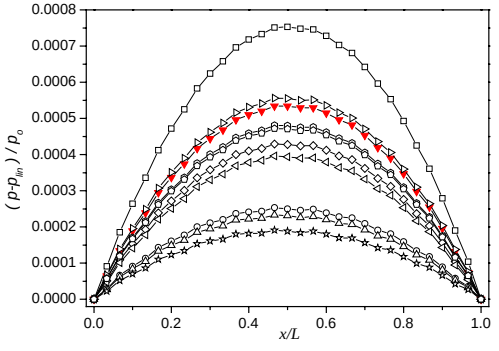

(b)

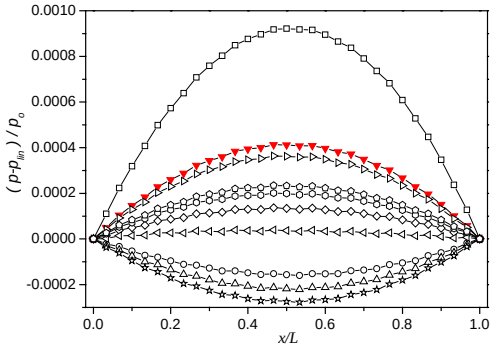

(c)

Fig. 5. Deviations from linear pressure drop at $\Pi = 1.1$. Here ▼ indicates the results of DSMC method, □ indicates the results of Beskok and Karniadakis's model, ▷ indicates the results of Maxwell's model, ⬠ indicates the results of Sreekanth's model, ⬡ indicates the results of Mitsuya's model, ◇ indicates the results of Hadjiconstantniou's model, ◁ indicates the results of Hisa and Domoto's model, ◯ indicates the results of Cercignani's model, Δ indicates the results of Deissler's model, and ☆ indicates the results of Schamberg's model. (a) $Kn = 0.1$, (b) $Kn = 0.2$ and (c) $Kn = 0.4$.

curvature while the model of Beskok and Karniadakis with the lowest second-order coefficient gives the largest curvature. The pressure distributions obtained by Sreekanth's model and Mitsuya's model lie intermediately among all the slip models and are close to the DSMC results, which are indicated by the inverted closed triangles in Fig. 5.

To validate the curve surface, we can obtain similar expressions for a circular microtube with diameter D and length L in the fully-developed flow regime:

$$u = \frac{D^2}{16\eta}\frac{dp}{dx}\left(\frac{r^2}{(D/2)^2} - 1 - 4C_1Kn - 8C_2Kn^2\right), \tag{13}$$

$$u_A = -\frac{D^2}{32\eta}\frac{dp}{dx}(1 + 8C_1Kn + 16C_2Kn^2), \tag{14}$$

$$\frac{u}{u_A} = \frac{2 - 8r^2/D^2 + 8C_1Kn + 16C_2Kn^2}{1 + 8C_1Kn + 16C_2Kn^2}, \tag{15}$$

$$Q_A = \frac{u_A}{-((D/2)/p)(dp/dx)\sqrt{(RT/2)}} = \frac{\sqrt{\pi}(1 + 8C_1Kn + 16C_2Kn^2)}{16Kn}, \tag{16}$$

$$C_f = \frac{\tau_w}{\rho u_A^2/2} = \frac{16}{\mathrm{Re}(1 + 8C_1Kn + 16C_2Kn^2)} = \frac{\sqrt{\pi}}{\mathrm{Re}KnQ_A}, \tag{17}$$

$$\dot{m} = \rho h u_A = \frac{p_0^2 D^4}{256RT\eta L}(\Pi^2 - 1 + 16C_1Kn_0(\Pi - 1) + 32C_2Kn_0^2 \ln\Pi), \tag{18}$$

$$P^2 - \Pi^2 + 16C_1Kn_0(P - \Pi) - 32C_2Kn_0^2 \ln\left(\frac{\Pi}{P}\right) - [1 - \Pi^2 + 16C_1Kn_0(1 - \Pi) - 32C_2Kn_0^2 \ln\Pi]\frac{x}{L} = 0, \tag{19}$$

where the Knudsen number is defined as $Kn = \lambda/D$, and Reynolds number is defined as $\mathrm{Re} = \rho u_A D/\eta$. We only show the flow rate in Fig. 6 due to the space limitation. We can see that the results are similar with those in a plane channel. The predictions from Sreekanth' model ($C_2 = 0.14$), followed by Mitsuya's model ($C_2 = 2/9$), also agree well with the linearized Boltzmann solutions up to $Kn = 2$, while other slip models can give good agreement only for $Kn < 0.1$.

4. Conclusions

Analytical solutions for the simplified Navier–Stokes equation with various first-order and second-order slip boundary conditions are presented in this paper. Comparisons for velocity profile, flow rate, friction factor, and pressure distribution predicted from various slip models are performed and the following conclusions are made.

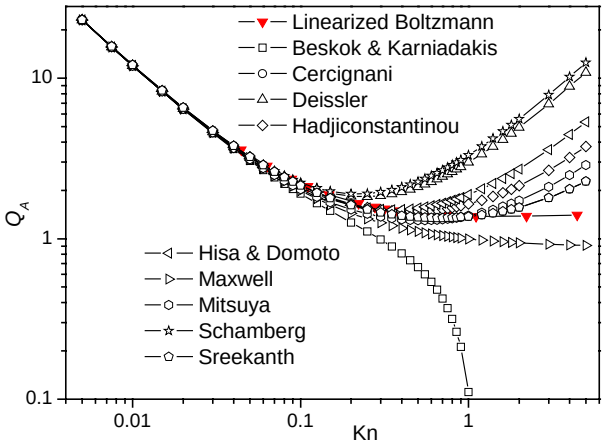

Fig. 6. Comparison of non-dimensional flow rate Q_A resulting from each slip model for a circular tube.

(1) For slip velocity at wall, the first-order coefficient dominates the slip velocity for lower Knudsen numbers while the second-order coefficient plays a more important role for higher Knudsen numbers. The model of Beskok and Karniadakis with the smallest second-order coefficient gives the best agreement with the linearized Boltzmann solutions while Cercignani's model, Hadjiconstantinou's model and Schamberg's model perform the worst in the present Knudsen number range.

(2) For the centerline velocity, Maxwell's model and Beskok and Karniadakis's model give the most accurate description while Cercignani's model and Schamberg's model perform the worst. The slip models with positive second-order slip coefficients ($C_2 > 0$) under-estimate centerline velocity while the slip model with negative second-order slip coefficient ($C_2 < 0$) over-estimates the centerline velocity.

(3) For flow rate and friction factor, various slip models are in rough agreement with the linearized Boltzmann solutions for $Kn < 0.1$. But Sreekanth's model, followed by Mitsuya's model, gives a good agreement from the slip regime ($0.001 < Kn < 0.1$) up to $Kn = 2$.

(4) The second-order coefficient has significant effect on pressure distribution. The pressure curvature deviating from the linear pressure distribution of corresponding incompressible flows increases as the second-order coefficient decreases. In a whole the pressure distributions from Sreekanth's model and Mitsuya's model are very close to the solutions of the DSMC method.

In summary, in situations where the flow rate and friction factor are of interest, Sreekanth's model is suggested to be adopted from slip regime up to $Kn = 2$, followed by Mitsuya's model. As for the velocity profile, the predictions of Sreekanth's model and Mitsuya's model lie intermediately among the various slip models shown

in Table 1. Rather, the pressure distributions obtained by Sreekanth's model and Mitsuya's model also lie intermediately among all the slip models and are very close to the DSMC results. Moreover, Sreekanth reports a good agreement of the model with his experimental results (including mass flow rate, pressure drops and cross-sectional velocity) for Knudsen number as high as $Kn = 1.5$.[15] The other first-order or second-order slip models shown in Table 1 are limited to slip regime or marginally transition regime and break down around $Kn = 0.1$. This study also suggests that when one compares his experimental data with slip models, one must pay attention to the Knudsen number range and choose proper slip model. It is worth noticing that Sun *et al.*[48] also proposed new first-order and second-order slip coefficients by incorporating VHS and VSS molecular dynamics. However, their simulation results show that the model is only comparable to Mitsuya's model. However, it is worth noticing that the momentum accommodation coefficient σ_ν was not involved in this paper. The momentum accommodation coefficient is defined as the fraction of molecules reflected diffusively at wall. This coefficient depends on the fluid, the solid and the surface finish. In the above two recommended slip models, the momentum accommodation coefficient was taken into account in Mitsuya's model by multiplying $(2 - \sigma_\nu)/\sigma_\nu$ before the first term in the right-hand side of Eq. (2) but it was not considered in Sreekanth's model.

Besides the often-used second-order slip condition like Eq. (2), some authors attempted to provide a general model in the slip and transition regime by introducing an expression of Knudsen number, e.g., a hyperbolic tangent function of Knudsen number[49] or an empirical parameter,[50] in the power series of velocity distribution function and slip boundary conditions. One can refer to Refs. 49 and 50 for further details.

Acknowledgments

This work was supported by the National Natural Science Foundation of China (No. 50406020).

References

1. G. E. Karniadakis and A. Beskok, *Micro Flows*: *Fundamentals and Simulation* (Springer-Verlag, New York, 2001).
2. P. Y. Wu and W. A. Little, *Cryogenics* **23**, 273 (1983).
3. J. Pfahler, J. Harley, H. H. Bau and J. N. Zemel, *ASME*, *DSC* **32**, 49 (1991).
4. S. B. Choi, R. F. Barron and R. O. Warrington, *ASME*, *DSC* **32**, 123 (1991).
5. S. E. Turner, H. W. Sun and M. Faghri, *ASME*, *HTD* **364-3**, 71 (1999).
6. E. Kennard, *Kinetic Theory of Gases* (McGraw-Hill, New York, 1938).
7. A. Burgdorfer, *ASME J. Basic Eng.* **81**, 94 (1959).
8. W. A. Ebert and E. M. Sparrow, *ASME J. Basic Eng.* **87**, 1018 (1965).
9. E. B. Arkilic, M. A. Schmidt and K. S. Breuer, *J. Microelectromechanical Systems* **6**, 167 (1997).
10. G. L. Morini and M. Spiga, *Microscale Thermophys. Eng.* **2**, 273 (1998).
11. H. Sun and M. Faghri, *ASME J. Fluids Eng.* **122**, 440 (2000).

12. R. Schamberg, The fundamental differential equations and the boundary conditions for high speed slip-flow, and their application to several specific problems, PhD thesis, California Institute of Technology, 1947.
13. C. Cercignani, *Institute of Engineering Research Report AS-64-19* (University of California, Berkeley, 1964).
14. R. G. Deissler, *Int. J. Heat Mass Transfer* **7**, 681 (1964).
15. A. K. Sreekanth, *6th Int. Symp. on Rarefied Gas Dynamics* (1969), p. 667.
16. Y. T. Hisa and G. A. Domoto, *ASME J. Lubrication Technology* **105**, 120 (1983).
17. Y. Mitsuya, *J. Tribol.* **115**, 289 (1993).
18. A. Beskok and G. E. Karniadakis, *ASME J. Fluids Eng.* **118**, 448 (1996).
19. C. Aubert and S. Colin, *Microscale Thermophysical Eng.* **5**, 41 (2001).
20. N. G. Hadjiconstantinou, *Phys. Fluids* **15**, 2352 (2003).
21. J. Maurer, P. Tabeling, P. Joseph and H. Willaime, *Phys. Fluids* **15**, 2613 (2003).
22. J. Maurer, P. Tabeling, P. Joseph and H. Willaime, *Numerical Heat Transfer Part A* **32**, 677 (1997).
23. J. Dai, D. Xu, B. C. Khoo and K. Y. Lam, *J. Micromech. Microeng.* **10**, 372 (2000).
24. C. S. Chen, S. M. Lee and J. D. Sheu, *Numerical Heat Transfer Part A* **33**, 749–762 (1998).
25. H. Z. Zhao, *Int. Comm. Heat Mass Transfer* **18**, 585 (2001).
26. S. Roy and R. Raju, *J. Applied Phys.* **93**, 4870 (2003).
27. Y. Asako, T. Q. Pi, S. E. Turner and M. Faghri, *Int. J. Heat Mass Transfer* **46**, 3041 (2003).
28. C. S. Chen, *Int. J. Computer Applications in Technology* **13**, 316 (2000).
29. C. S. Chen, *J. Micromech. Microeng.* **14**, 1091 (2004).
30. H. Xue, H. M. Ji and C. Shu, *Int. J. Heat Mass Transfer* **44**, 4139 (2001).
31. H. Xue, H. M. Ji and C. Shu, *Microscale Thermophysical Eng.* **7**, 51 (2003).
32. D. X. Du and K. Suzuki, *J. Turbulence* **5**, 21 (2004).
33. X. B. Nie, G. D. Doolen and S. Y. Chen, *J. Stat. Phys.* **107**, 279 (2002).
34. C. Y. Lim, C. Shu, X. D. Niu and Y. T. Chew, *Phys. Fluids* **14**, 2299 (2002).
35. G. H. Tang, W. Q. Tao and Y. L. He, *Int. J. Mod. Phys. C* **15**, 335 (2004).
36. G. H. Tang, W. Q. Tao and Y. L. He, *Phys. Fluids* **17**, 058101 (2005).
37. M. Sbragaglia and S. Succi, *Phys. Fluids* **17**, 093602 (2005).
38. R. Benzi, L. Biferale, M. Sbragaglia, S. Succi and F. Toschi, *J. Fluid Mechanics* **548**, 257 (2006).
39. C. Cercignani, *The Boltzmann Equation and Its Applications* (Springer-Verlag, New York, 1988).
40. T. Ohwada, Y. Sone and K. Aoki, *Phys. Fluids A* **1**, 2042 (1989).
41. S. K. Loyalka and S. A. Hamoodi, *Phys. Fluids A* **2**, 2061 (1990).
42. P. L. Bhatnangar, E. P. Gross and M. Krook, *Phys. Rev.* **94**, 511 (1954).
43. G. A. Bird, *Molecular Gas Dynamics and the Direct Simulation of Gas Flows* (Clarendon Press, Oxford, 1994).
44. N. G. Hadjiconstantinou and O. Simek, *ASME J. Heat Transfer* **124**, 356 (2002).
45. E. B. Arkilic, K. S. Breuer and M. A. Schmidt, *ASME, FED* **197**, 57 (1994).
46. E. B. Arkilic, K. S. Breuer and M. A. Schmidt, *J. Fluid Mech.* **437**, 29 (2001).
47. J. C. Shih, C. M. Ho, J. Q. Liu and Y. C. Tai, *ASME, DSC* **59**, 197 (1966).
48. Y. H. Sun, W. K. Chan and N. Y. Liu, *J. Micromech. Microeng.* **12**, 316 (2002).
49. H. Xue and Q. Fan, *Microscale Thermophysical Eng.* **4**, 125 (2000).
50. A. Beskok and G. E. Karniadakis, *Microscale Thermophysical Eng.* **3**, 43 (1999).